Geophys. J. Int. (2008) **174,** 1037–1051 doi: 10.1111/j.1365-246X.2008.03896.x

Formulation of the multiple anisotropic scattering process in two dimensions for anisotropic source radiation

Eduard Carcolé[1] and Arantza Ugalde[2]

[1]*Universitat Politècnica de Catalunya, Dept. Enginyeria del Terreny, Cartogràfica i Geofísica, Jordi Girona* 1-3*, Edifici* D2, 08034 *Barcelona, Spain.*
E-mail: eduard.carcole@upc.edu
[2]*Observatori de l'Ebre, Horta Alta* 38, 43520 *Roquetes, Spain*

Accepted 2008 June 24. Received 2008 June 16; in original form 2007 October 15

SUMMARY

The radiative transfer theory (RTT) describes the energy transport through a random heterogeneous medium, neglecting phase information. It provides an adequate framework for modelling high-frequency seismogram envelopes. For isotropic scattering and sources, the radiative transfer equation (RTE) has been formulated analytically and numerically simulated using Monte Carlo methods for acoustic and elastic media. Here, we derive an exact analytical solution of the RTE in 2-D space for the acoustic case, including anisotropic scattering for a anisotropic point-like impulsive source. For this purpose, we generalize the path integral method, which has been used before in the isotropic case, to take into account the anisotropy of both the source radiation pattern and scattering processes, simultaneously. Then we obtain a general solution, which is written in a closed form in the Fourier space. To illustrate the theoretical results, we compute the full space and time evolution of the specific intensity for an arbitrary case. We also compare the time traces computed from our general solution with cases in which the source and/or the scattering process are isotropic. The importance of taking into account both anisotropies simultaneously becomes obvious in our examples. We also show that at long lapse time, our example approaches the solution of the diffusion equation.

Key words: Seismic attenuation; Wave scattering and diffraction; Wave propagation.

1 INTRODUCTION

It has become widely accepted that coda waves of local earthquakes are the product of the scattering process caused by small-scale random heterogeneities of the lithosphere. There have been a number of approaches to model coda envelope shapes. Early work (Aki & Chouet 1975) modelled the coda as singly scattered waves in a uniform medium. *S*-coda envelopes have been extensively studied by using this first-order model, which is valid at short lapse times. However, as lapse time increases, a greater contribution of multiple scattering is expected. The multiple scattering process has been formulated on the basis of the radiative transfer theory (RTT) for the energy density. The radiative transfer (or Boltzmann) equation (RTE) is a basic analytical tool in other fields as nuclear reactor theory, the kinetic theory of gases or in electron transport through conducting materials. It describes the propagation of energy and transport of matter through random scattering media by neglecting phase information (Chandrasekhar 1960; Ishimaru 1978; Rytov *et al.* 1987). RTT works well if the typical scale length of the heterogeneities and wavelength are of comparable size and if medium fluctuations are moderate (Ryzhick *et al.* 1996). The stationary-state solution of the RTE for isotropic scattering was first introduced into seismology by Wu (1985) and Wu & Aki (1988) to model the high frequency seismogram envelopes of local earthquakes. Shang & Gao (1988) formulated the 2-D multiple isotropic scattering process for the non-stationary state and impulsive spherical source radiation. Zeng *et al.* (1991) extended the formulation to the 3-D space for the case of isotropic scattering of acoustic waves, thus neglecting the vector nature of elastic waves and conversions between *P* and *S* waves. Under the same assumptions, Paasschens (1997) found an approximate analytical solution of the RTE, using the interpolation between exact solutions for the 2-D and 4-D cases. Sato (1994, 1995) formulated the multiple anisotropic scattering process in 2-D and 3-D, respectively. Sato *et al.* (1997) investigated the multiple isotropic scattering process for non-spherical source radiation. In parallel with the analytical ones, numerical studies based on the Monte Carlo method have been developed to solve the RTE in acoustic and elastic media (e.g. Gusev & Abubakirov 1987; Hoshiba 1991; Hoshiba 1995; Margerin *et al.* 2000; Yoshimoto 2000; Przybilla *et al.* 2006).

As pointed out by several observations and theoretical developments (e.g. Gusev & Abubakirov 1987; Hoshiba 1995; Sato 1995), understanding the anisotropic scattering process is important in studies of coda waves and seismic wave attenuation. Scattering is anisotropic in the real Earth, and it depends on frequency. In particular, evidence for the invalidness of the hypothesis of isotropic scattering in the Earth

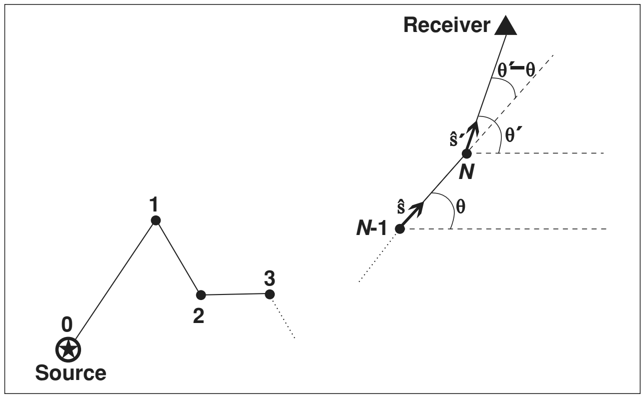

Figure 1. Schematic plot of the anisotropic scattering process in 2-D.

is the direct wave pulse broadening with propagation distance (see Sato & Fehler 1998), which contradicts the prediction of the isotropic scattering model in which the pulse width remains constant (Abubakirov 2005). This property of seismic waves is considered to be caused by multiple forward scattering and diffraction by random heterogeneities (Takahashi *et al.* 2007). Moreover, it has long been observed that the early coda of local earthquakes, immediately after the direct wave arrival, reflects the effects of the source radiation pattern, although the dependence on directivity diminishes as lapse time increases (Sato *et al.* 1997). Most studies of coda envelopes have used the isotropic scattering and spherical radiation pattern assumptions to account for observations. By introducing in the theoretical models the anisotropy of scattering and the radiation pattern correction, we will be able to perform more accurate analysis.

Analytical solutions of the RTE for a medium with anisotropic radiation pattern of the source and anisotropy of scattering incorporated simultaneously, have not been found yet. In this paper, we derive an exact analytical solution of the RTE for the acoustic case in 2-D space, assuming both anisotropic scattering processes and anisotropic point-like impulsive source. We also assume that the absorption of the media is constant and scattering properties of the media are statistically uniform. This general solution is written in a closed form in the Fourier space.

2 THE ACOUSTIC RADIATIVE TRANSFER EQUATION

The RTE describes the position $\mathbf{r}$ and time t dependence of the specific intensity $I(\mathbf{r}, t, \hat{\mathbf{s}})$, being the energy flux per unit angle at position $\mathbf{r}$ and time t, in the direction $\hat{\mathbf{s}}$ (Fig. 1). Its time evolution in 2-D space is governed by the following equation (Ishimaru 1978)

$$\left(\frac{1}{v}\frac{\partial}{\partial t} + \hat{\mathbf{s}}\cdot\nabla + l^{-1}\right) I(\mathbf{r}, t, \hat{\mathbf{s}}) = \frac{l^{-1}}{2\pi}\int f(\hat{\mathbf{s}}|\hat{\mathbf{s}}')I(\mathbf{r}, t, \hat{\mathbf{s}}')\mathrm{d}\hat{\mathbf{s}}' + v^{-1}S(\mathbf{r}, t, \hat{\mathbf{s}}), \tag{1}$$

and the angular average of the specific intensity is

$$\overline{I}(\mathbf{r}, t) = \frac{1}{2\pi}\int I(\mathbf{r}, t, \hat{\mathbf{s}})\mathrm{d}\hat{\mathbf{s}}. \tag{2}$$

In eq. (1), S is the source term, v is the velocity of the energy, l is the mean free path for scattering and f is the dimensionless quantity called the phase function in RTT. Function f describes the wave intensity transfer from a direction $\hat{\mathbf{s}}$ into a direction $\hat{\mathbf{s}}'$ (Fig. 1). Since absorption is independent of $\mathbf{r}$ and $\hat{\mathbf{s}}$, and it is taken into account through a multiplicative factor exp $(-l_a vt)$, where l_a is absorption length; here it is not considered.

In random media, the phase function is usually estimated in the Born approximation (Born & Wolf 2002). In such conditions f is only a function of $|\hat{\mathbf{s}} - \hat{\mathbf{s}}'|$, and it can be computed from the autocorrelation function of the inhomogeneity field, assumed to be statistically uniform (Gusev & Abubakirov 1996; Sato & Fehler 1998). Function f in eq. (1) is related to a normalized scattering radiation pattern or 'indicatrix' function ϕ (Gusev & Abubakirov 1996; Rytov *et al.* 1987) by

$$\frac{1}{2\pi} f(\hat{\mathbf{s}}|\hat{\mathbf{s}}') = \phi\left(\theta' - \theta\right), \tag{3}$$

where θ and θ' are the angles of the unit vectors $\hat{\mathbf{s}}$ and $\hat{\mathbf{s}}'$, respectively (Fig. 1), and ϕ verifies the normalization condition $\int_0^{2\pi}\phi(\theta' - \theta)\mathrm{d}\theta' = 1$.

Eq. (1) has been solved analytically in 2-D for both $I(\mathbf{r}, t, \hat{\mathbf{s}})$ and total intensity $\overline{I}(\mathbf{r}, t)$, by assuming a point-like spherical source and isotropic scattering (Paasschens 1997). The solution for $\overline{I}(\mathbf{r}, t)$ reads

$$\overline{I}(\mathbf{r}, t) = \exp(-t/\tau)\left[\frac{\delta\,(r - vt)}{2\pi r} + \frac{1}{2\pi l\sqrt{v^2t^2 - r^2}}\exp\left(l^{-1}\sqrt{v^2t^2 - r^2}\right)H\,(vt - r)\right], \tag{4}$$

where $H(x)$ is the Heaviside step function and $\tau = l/v$ is the mean free time between scattering events. This expression was previously obtained by Sato (1994) by performing a Fourier-Laplace analysis of the RTE. Later, Sato (1994) showed that a Fourier–Laplace analysis leads to a system of equations that allows obtaining solutions for $I(\mathbf{r}, t)$ in 2-D for the case of anisotropic scattering.

The aim of this paper is to obtain exact analytical solutions of (1) for both $I(\mathbf{r}, t, \hat{\mathbf{s}})$ and $\overline{I}(\mathbf{r}, t)$, assuming a 2-D space, an arbitrary anisotropic point-like impulsive source and an arbitrary phase function that depends on the relative angle between the directions of the vectors $\hat{\mathbf{s}}$ and $\hat{\mathbf{s}}'$ before and after the collision.

3 COMPACT INTEGRAL EXPRESSION FOR THE RTE IN 2-D FOR ANISOTROPIC SCATTERING AND SOURCE RADIATION

Our final objective is to derive the exact solution of (1) in the Fourier space, by using a path integral method, which has allowed solving the RTE in two, three and four dimensions for isotropic source and scattering. For this purpose, we first derive an integral expression from (1) following Paasschens (1997) but taking into account the anisotropy of both the source and the scattering events.

We consider separately the contributions to the specific intensity from $N = 0, 1, 2, \ldots,$ scattering events. Then:

$$I(\mathbf{r}, t, \hat{\mathbf{s}}) = \sum_{N=0}^{\infty} I(\mathbf{r}, t, \hat{\mathbf{s}}, N), \quad \overline{I}(\mathbf{r}, t) = \sum_{N=0}^{\infty} \overline{I}(\mathbf{r}, t, N). \tag{5}$$

The partial intensities $I(\mathbf{r}, t, \hat{\mathbf{s}}, N)$ satisfy (Paasschens 1997)

$$\left(\frac{1}{v}\frac{\partial}{\partial t} + \hat{\mathbf{s}}_N \cdot \nabla + l^{-1}\right) I(\mathbf{r}, t, \hat{\mathbf{s}}_N, N) = l^{-1} \int f_N(\hat{\mathbf{s}}_N|\hat{\mathbf{s}}_{N-1}) I(\mathbf{r}, t, \hat{\mathbf{s}}_{N-1}, N-1) \frac{\mathrm{d}\hat{\mathbf{s}}_{N-1}}{2\pi}, \quad N > 0,$$

$$\left(\frac{1}{v}\frac{\partial}{\partial t} + \hat{\mathbf{s}}_0 \cdot \nabla + l^{-1}\right) I(\mathbf{r}, t, \hat{\mathbf{s}}_0, 0) = v^{-1} S(\mathbf{r}, t, \hat{\mathbf{s}}_0), \tag{6}$$

where $f_N(\hat{\mathbf{s}}_N|\hat{\mathbf{s}}_{N-1})$ is the phase function of the Nth scattering event. According to eq. (1), we have

$$f_N(\hat{\mathbf{s}}_N|\hat{\mathbf{s}}_{N-1}) = f(\hat{\mathbf{s}}_N|\hat{\mathbf{s}}_{N-1}), \quad N > 0. \tag{7}$$

The case $N = 0$ takes into account the anisotropy of the source. To integrate (6), we note that the differential operator in the left-hand side corresponds to the total variation of $I(\mathbf{r}, t, \hat{\mathbf{s}}_N, N)$ along the direction of energy propagation (indicated by $\hat{\mathbf{s}}_N$) at the position $\mathbf{r}$ after the Nth scattering event. Then, following a notation similar to Chandrasekhar (1960, p. 8) we may write the total variation as

$$\left(\frac{1}{v}\frac{\partial}{\partial t} + \hat{\mathbf{s}}_N \cdot \nabla\right) = \frac{\mathrm{d}}{\mathrm{d}s_N}. \tag{8}$$

Then (6) becomes

$$\left(\frac{\mathrm{d}}{\mathrm{d}s_N} + l^{-1}\right) I(\mathbf{r}, t, \hat{\mathbf{s}}_N, N) = l^{-1} \int f_N(\hat{\mathbf{s}}_N|\hat{\mathbf{s}}_{N-1}) I(\mathbf{r}, t, \hat{\mathbf{s}}_{N-1}, N-1) \frac{\mathrm{d}\hat{\mathbf{s}}_{N-1}}{2\pi}, \quad N > 0,$$

$$\left(\frac{\mathrm{d}}{\mathrm{d}s_0} + l^{-1}\right) I(\mathbf{r}, t, \hat{\mathbf{s}}_0, 0) = v^{-1} S(\mathbf{r}, t, \hat{\mathbf{s}}_0). \tag{9}$$

The integration is now readily performed by integrating s_N on a half line given by $\mathbf{r}$ and $\hat{\mathbf{s}}_N$ from $-\infty$ up to current location $\mathbf{r}$ (Chandrasekhar 1960, Chapter 1, pp. 9-10). Writing the integral in terms of r_N we obtain

$$I(\mathbf{r}, t, \hat{\mathbf{s}}_N, N) = \int\int \frac{\mathrm{d}\hat{\mathbf{s}}_{N-1}}{2\pi} \mathrm{d}r_N\, p(r_N) f_N(\hat{\mathbf{s}}_N|\hat{\mathbf{s}}_{N-1}) I(\mathbf{r} - r_N\hat{\mathbf{s}}_N, t - r_N/v, \hat{\mathbf{s}}_{N-1}, N-1), \; N > 0,$$

$$I(\mathbf{r}, t, \hat{\mathbf{s}}_0, 0) = \tau \int \mathrm{d}r_0\, p(r_0) S(\mathbf{r} - r_0\hat{\mathbf{s}}_0, t - r_0/v, \hat{\mathbf{s}}_0), \tag{10}$$

where we have defined

$$p(r_N) = l^{-1} \exp(-r_N/l), \tag{11}$$

and the source term is written as

$$S(\mathbf{r}, t, \hat{\mathbf{s}}_0) = f_0(\hat{\mathbf{s}}_0|\hat{\mathbf{s}}_{-1}) \delta(\mathbf{r}) \delta(t). \tag{12}$$

Function $f_0(\hat{\mathbf{s}}_0|\hat{\mathbf{s}}_{-1})$ is an arbitrary function, which takes into account the anisotropic emission of energy and $\hat{\mathbf{s}}_{-1}$ is a constant unit vector, taking into account the orientation of the source. Using the source term (12) in eq. (10), we can give the explicit expression for the ballistic intensities ($N = 0$):

$$I(\mathbf{r}, t, \hat{\mathbf{s}}_0, 0) = \exp(-t/\tau) f_0(\hat{\mathbf{s}}_0|\hat{\mathbf{s}}_{-1}) \delta(\mathbf{r} - vt\hat{\mathbf{s}}_0). \tag{13}$$

Solving the recursive relations in (10), we obtain an integral expression for $I(\mathbf{r}, t, \hat{\mathbf{s}}_N, N)$

$$I(\mathbf{r}, t, \hat{\mathbf{s}}_N, N) = \tau \int \mathrm{d}r_0 \ldots \int \mathrm{d}r_N \int \frac{\mathrm{d}\hat{\mathbf{s}}_0}{2\pi} \ldots \int \frac{\mathrm{d}\hat{\mathbf{s}}_{N-1}}{2\pi} \left[\prod_{i=0}^{N} p(r_i) f_i(\hat{\mathbf{s}}_i|\hat{\mathbf{s}}_{i-1})\right] \delta\left(t - \sum_{i=0}^{N} \frac{r_i}{v}\right) \delta(\mathbf{r} - \sum_{i=0}^{N} r_i\hat{\mathbf{s}}_i). \tag{14}$$

Note that (14) holds for $N = 0$. Then, a single integral over r_0 has to be performed. We could also have considered the summation over all N in eq. (10), thus resulting in the following integral equation:

$$I(\mathbf{r}, t, \hat{\mathbf{s}}) = I(\mathbf{r}, t, \hat{\mathbf{s}}, 0) + \int\int \frac{\mathrm{d}\hat{\mathbf{s}}'}{2\pi} \mathrm{d}r'\, p(r') f(\hat{\mathbf{s}}|\hat{\mathbf{s}}') I(\mathbf{r} - r'\hat{\mathbf{s}}, t - r'/v, \hat{\mathbf{s}}'). \tag{15}$$

Usually, the Fourier–Laplace transform of (15) or similar integral equations are considered to obtain analytical expressions for $\overline{I}(\mathbf{r}, t)$. However, that kind of analysis did not allow obtaining analytical solutions in a general case (non-spherical source radiation and anisotropic scattering).

4 SOLUTION OF THE RADIATIVE TRANSFER EQUATION IN 2-D FOR ANISOTROPIC SOURCE AND SCATTERING EVENTS

We will show that (14) may be solved analytically in the 2-D Fourier space. Rewriting the integral in (14) in terms of the angles θ_i of the vectors $\hat{\mathbf{s}}_i$ and rearranging terms we obtain

$$I(\mathbf{r}, t, \theta_N, N) = \tau \prod_{i=0}^{N} \int_0^{\infty} \mathrm{d}r_i\, p(r_i) \delta \left(t - \sum_{i=0}^{N} \frac{r_i}{v} \right) \times \left[2\pi \int_0^{2\pi} \mathrm{d}\theta_0 ... \int_0^{2\pi} \mathrm{d}\theta_{N-1} \prod_{j=0}^{N} \phi_j \left(\theta_j - \theta_{j-1} \right) \delta(x - \sum_{i=0}^{N} r_i \cos\theta_i) \delta \left(y - \sum_{i=0}^{N} r_i \sin\theta_i \right) \right], \tag{16}$$

where $\phi_j \left(\theta_j - \theta_{j-1} \right) = \left(1/2\pi \right) f_j(\hat{\mathbf{s}}_j | \hat{\mathbf{s}}_{j-1})$, according to (3).

We will solve (16) in two steps. First, we will solve the integrals over the angles (the part inside the square bracket). For this purpose, we note here that the functions ϕ_j are periodic. By using a Fourier series expansion, we may write

$$\phi_j \left(\theta_j - \theta_{j-1} \right) = \frac{1}{2\pi} \sum_{n_j} A_{n_j} \mathrm{e}^{\mathrm{i} n_j \left(\theta_j - \theta_{j-1} \right)}, \tag{17}$$

where the Fourier coefficients A_{n_j} are complex numbers in a general case. Note that in a general case n_j goes from $-\infty$ to ∞, but for practical purposes it will be necessary to write or approximate ϕ_j by considering a finite number of terms. For $j = 0$, we have $\phi_0 \left(\theta_0 - \theta_{-1} \right)$ where θ_{-1} is a constant angle that takes into account the orientation of the source. For the sake of simplicity, we will choose the orientation of the x-axis in such a way that $\theta_{-1} = 0$. In a second step, the whole integral will be solved. The integration is carried out in the Appendix. We obtain

$$I(\mathbf{r}, t, \theta_N, N) = \frac{1}{(2\pi)^3} \int_{-\infty}^{\infty} \mathrm{e}^{\mathrm{i}\omega t} \mathrm{d}\omega \int_0^{\infty} \xi \mathrm{d}\xi \int_{-\pi}^{\pi} \mathrm{d}\varphi \mathrm{e}^{\mathrm{i}\xi r \cos(\theta - \varphi)} \tilde{I}(\xi, \omega, \theta_N, N), \tag{18}$$

where the pair $\xi = (\xi, \varphi)$ are the radial and angular coordinates in the Fourier space. $\tilde{I}(\xi, \omega, \theta_N, N)$ is the Fourier transform of $I(\mathbf{r}, t, \theta_N, N)$, and it is given by

$$\begin{aligned} &\tilde{I}(\xi, \omega, \theta_0, N = 0) = \tau \sum_{n_0} E_{n_0}(\xi, \omega, \theta_0), \\ &\tilde{I}(\xi, \omega, \theta_N, N) = \tau \sum_{n_0, \ldots, n_N} \prod_{k=0}^{N-1} C_{n_k - n_{k+1}}(\xi, \omega) E_{n_N}(\xi, \omega, \theta_N), \quad N > 0 \end{aligned} \tag{19}$$

and

$$\begin{aligned} &E_{n_N}(\xi, \omega, \theta_N) = \frac{\tau^{-1} A_{n_N} \mathrm{e}^{\mathrm{i} n_N \theta_N}}{\tau^{-1} + \mathrm{i} \left[\omega + v\xi \cos(\theta_N - \varphi) \right]}, \\ &C_{n_j - n_{j+1}}(\xi, \omega) = A_{n_j} \mathrm{e}^{\mathrm{i}(n_j - n_{j+1})(\varphi - \pi/2)} D_{n_j - n_{j+1}}(\xi, \omega) \end{aligned} \tag{20}$$

where the function D_n is defined as

$$\begin{aligned} &D_n(\xi, \omega) = \tau^{-1} \frac{\left[\sqrt{(\tau^{-1} + \mathrm{i}\omega)^2 + v^2 \xi^2} - \left(\tau^{-1} + \mathrm{i}\omega \right) \right]^n}{v^n \xi^n \sqrt{\left(\tau^{-1} + \mathrm{i}\omega \right)^2 + v^2 \xi^2}}, \quad n > -1 \\ &D_{-n}(\xi, \omega) = (-1)^n D_n(\xi, \omega), \qquad n < 0. \end{aligned} \tag{21}$$

Now we have to compute

$$\tilde{I}(\xi, \omega, \Theta) = \sum_{N=0}^{\infty} \tilde{I}(\xi, \omega, \Theta, N), \tag{22}$$

where $\Theta = \theta_0 = \theta_1 = ... = \theta_N$ is the angle of $\hat{\mathbf{s}}$ in (5). To compute eq. (22), it is very important to note that eq. (19) has a structure that corresponds to a product of a certain number of matrices times a vector. To show more clearly this structure, let us rewrite $\tilde{I}(\xi, \omega, \Theta, N)$ for $N > 0$ in the following way

$$\tilde{I}(\xi, \omega, \Theta, N) = \tau \sum_{n_0} \left(\sum_{n_1} C_{n_0 - n_1} \cdots \left(\sum_{n_{N-1}} C_{n_{N-2} - n_{N-1}} \left(\sum_{n_N} C_{n_{N-1} - n_N}(\xi, \omega) E_{n_N}(\xi, \omega, \Theta) \right) \right) \cdots \right). \tag{23}$$

Note than the innermost parentheses corresponds to the product of a vector $\mathbf{E}_N$ whose components are $E_{n_N}(\xi, \omega, \Theta)$ with a square matrix $\mathbf{C}_{N-1}$ whose components are $C_{n_{N-1}-n_N}(\xi, \omega)$ (n_{N-1} stands for rows and n_N stands for columns). Of course, the result of a matrix times a vector is another vector. Next parentheses correspond to the product of the resulting vector with a matrix $\mathbf{C}_{N-2}$ defined in an analogous way. Finally, the last summation over n_0 corresponds to the addition of the components of the vector resulting from all the products. Therefore, it is convenient to rewrite (22) using a 'vector-matrix' notation in the following way

$$\tilde{I}(\xi, \omega, \Theta) = \tau \sum_{n_0} u_{n_0}, \tag{24}$$

where u_{n_0} is the n_0 th component of a vector $\mathbf{u}$, which is obtained by the following relation

$$\mathbf{u} = \mathbf{E}_0 + \mathbf{C}_0 \cdot \mathbf{E}_1 + \mathbf{C}_0 \cdot \mathbf{C}_1 \cdot \mathbf{E}_2 + \mathbf{C}_0 \cdot \mathbf{C}_1 \cdot \mathbf{C}_2 \cdot \mathbf{E}_3 + ..., \tag{25}$$

and $\mathbf{C}_0$ is a matrix whose components are $C_{n_0-n_1}(\xi, \omega)$ (n_0 stands for rows and n_1 for columns). Note that $\mathbf{C}_0$ depends on the coefficients A_{n_0} (which define the anisotropy of the source radiation pattern) and it is not a square matrix in a general case. Note also that the vector $\mathbf{E}_0$, with components $E_{n_0}(\xi, \omega, \Theta)$, depends also on the coefficients A_{n_0}. Eq. (7) implies that all the matrices $\mathbf{C}_k$ for $k > 0$ are identical because A_{n_k} coincide for $k > 0$. Also all the vectors $\mathbf{E}_N$ for $N > 0$ are identical because A_{n_N} coincide for $N > 0$. Therefore, they will be denoted as $\mathbf{C} = \mathbf{C_k}$ and $\mathbf{E} = \mathbf{E_k}$ for $k > 0$, respectively. Taking into account equation (and using (25) we may rewrite eq. (22) as

$$\tilde{I}(\xi, \omega, \Theta) = \tau \sum_{n_0} u_{n_0} = \tau \sum_{n_0} \left[\mathbf{E}_0 + \mathbf{C}_0 \left(\sum_{k=0}^{\infty} \mathbf{C}^k \right) \mathbf{E} \right]_{n_0}. \tag{26}$$

Eq. (26) may be easily simplified. For this purpose, we define the matrix $\mathbf{S} = \sum_{k=0}^{\infty} \mathbf{C}^k$. This addition can be easily performed by noting that $\mathbf{S} \cdot \mathbf{C} = \mathbf{S} - \mathbf{I}$, where $\mathbf{I}$ is the identity matrix. Then we easily obtain $\mathbf{S} = (\mathbf{I} - \mathbf{C})^{-1}$. Finally, we may rewrite (26) as

$$\tilde{I}(\xi, \omega, \Theta) = \tau \sum_{n_0} \left(\mathbf{E}_0 + \mathbf{C}_0 \left(\mathbf{I} - \mathbf{C} \right)^{-1} \cdot \mathbf{E} \right)_{n_0}. \tag{27}$$

This is the main result of this paper. Note that the first term $\tau \sum_{n_0} (\mathbf{E}_0)_{n_0}$ in (27) is the Fourier transform of the ballistic term in eq. (13) and the second term takes into account multiple scattering. For $\bar{\tilde{I}}(\xi, \omega)$ we may write an analogous expression:

$$\bar{\tilde{I}}(\xi, \omega) = \tau \sum_{n_0} \left(\bar{\mathbf{E}}_0 + \mathbf{C}_0 \left(\mathbf{I} - \mathbf{C} \right)^{-1} \cdot \bar{\mathbf{E}} \right)_{n_0}, \tag{28}$$

where $\bar{\mathbf{E}}_0$ and $\bar{\mathbf{E}}$ are the corresponding angular averages of $\mathbf{E}$ and $\mathbf{E_0}$, which are given by

$$\bar{E}_{n_N}(\xi, \omega) = \frac{1}{2\pi} \int E_{n_N}(\xi, \omega, \Theta) \mathrm{d}\Theta = C_{n_N-0}. \tag{29}$$

Note that the function $\bar{E}_{n_N}$ can then be written as a function of $C_{n_N-n_{N+1}}$ where $n_{N+1} = 0$. If a finite number of Fourier coefficients are sufficient to describe the source and the scattering events, then eqs (27) and (28) become closed form solutions in the Fourier space. There is no simple way to invert eqs (27) and (28) or (19) in a general case to obtain analytical expressions for $I(\mathbf{r}, t, \mathbf{s})$ and $\bar{I}(\mathbf{r}, t)$, but numerical techniques exist to carry out 3-D Fourier transforms. This is further discussed in Section 5. Because the word 'inverse', in geophysics, is usually associated with backing out physical parameters from observations, to avoid confusion, we clarify that in the next we use the word 'inverse' for the back-transformation of the Fourier representation.

4.1 Derivation of $\bar{\tilde{I}}(\xi, \omega)$ for isotropic source and isotropic scattering

To finish our theoretical development, let us now obtain a known result from eq. (28). We may compute the angle averaged Fourier transform intensity $\bar{\tilde{I}}(\xi, \omega)$ for the case in which both the source and the scattering events are isotropic. In this case, all vectors and matrices have a single component. We immediately obtain

$$\bar{\tilde{I}}(\xi, \omega) = \tau \left[D_0(\xi, \omega) + \frac{D_0^2(\xi, \omega)}{1 - D_0(\xi, \omega)} \right] = \frac{1}{\sqrt{(\tau^{-1} + \mathrm{i}\omega)^2 + v^2\xi^2} - \tau^{-1}}, \tag{30}$$

which is the Fourier transform of eq. (4), and it can be obtained from Paasschens (1997, eq. 19).

5 A NUMERICAL EXAMPLE

We will illustrate now our results, and we will show the suitability of our theoretical expressions for carrying out numerical work, with an example. We consider a pulse of unit energy emitted at the origin of a 2-D frame. The source is anisotropic and defined by the function $\phi_0(\theta) = \pi^{-1} \cos^2 \theta$. The turn angle distribution for each scattering event will be described by an arbitrary function $\phi_j(\theta) = \phi(\theta) = \sum_{k=-8}^{8} A_k \exp(\mathrm{i}k\theta)$, for $j > 0$. The values for the coefficients A_k are chosen in Table 1 (we note here that ϕ_j are non-dimensional functions). The corresponding polar plot of the functions $\phi_0(\theta)$ and $\phi(\theta)$ is shown in Fig. 2. It is clearly observed that $\phi(\theta)$ is a anisotropic function in which forward scattering is more important than backscattering. Note that backscattering is mainly produced into two different directions. We have chosen this arbitrary function because its backscattering structure has some notable effects on the shape of $\bar{I}(\mathbf{r}, t)$.

Table 1. Fourier coefficients corresponding to the Fourier series expansion of $\phi(\theta)$ in Fig. 1(b)

Fourier coefficients	Value
A_0	1.0
$A_1 = A_{-1}$	2.109529×10^{-1}
$A_2 = A_{-2}$	4.068928×10^{-1}
$A_3 = A_{-3}$	5.622617×10^{-1}
$A_4 = A_{-4}$	3.99612×10^{-2}
$A_5 = A_{-5}$	2.17389×10^{-1}
$A_6 = A_{-6}$	1.13038×10^{-1}
$A_7 = A_{-7}$	-8.94269×10^{-3}
$A_8 = A_{-8}$	2.49811×10^{-2}

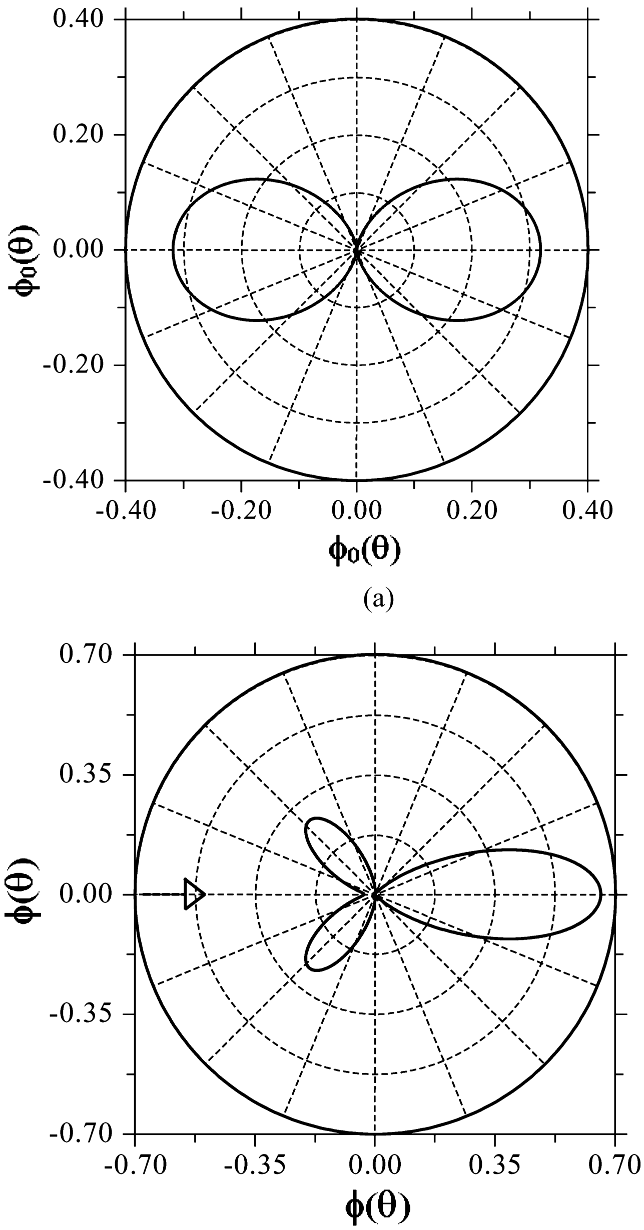

(b)

Figure 2. Polar plot of the functions (a) $\phi_0(\theta)$ and (b) $\phi(\theta)$. The arrow in (b) indicates the direction of the incident energy. Radial grid lines indicate sectors of 27.5°.

To carry out the inversion of $\bar{\tilde{I}}(\xi, \omega)$ [the same applies to $\tilde{I}(\xi, \omega, \Theta)$], we will use a 3-D FFT algorithm. Although the FFT algorithm has inaccuracy that it is difficult to establish in a general case and we could have used more accurate procedures, we will show that it provides a simple and fast tool to compute and visualize the space–time evolution of $\bar{I}(\mathbf{r}, t)$. The FFT algorithm does not diverge because of the ballistic term (which is the Fourier transform or the first term in eq. (28)), since its output is formally a linear combination of delta functions (Brigham 1998) separated by certain space and time intervals. This is a quite convenient property for 2-D graphical representations of $\bar{I}(\mathbf{r}, t)$, as we will immediately show.

To perform the calculations, we have to consider a maximum lapse time, which we write as $t_{\max}$. We would like to choose $t_{\max}$ such that we can visualize the evolution of $\bar{I}(\mathbf{r}, t)$ from a ballistic to diffusive behaviour. Then, we consider the mean square displacement derived by Boguna *et al.* (1996):

$$\langle r^2(t)\rangle = \frac{v^2}{\tau^{-2}(1-\psi)^2}[(1-\psi)\tau^{-1}t - 1 + \exp(-(1-\psi)\tau^{-1}t)], \tag{31}$$

where $\psi = \langle\cos\theta\rangle = \int_0^{2\pi}\phi(\theta)\cos\theta \mathrm{d}\theta$ is an anisotropic parameter, widely used in the literature (in our case $\psi \simeq 0.21$). In eq (31) there is a crossover time from a ballistic to diffusive behaviour, for a time of the order $\tau(1-\psi)^{-1}$. Then, in our calculations we considered $t_{\max} = 6\tau(1-\psi)^{-1} \simeq 7.60\tau$. This means that we compute a maximum lapse time, which corresponds to 7.60 times the mean free time. Also, to use the FFT algorithm, we have to consider a maximum extent for the length of both the x and y axes. We consider the maximum length for both the x and y axes to be 7.60 l.

To carry out the inversion, we used a 3-D FFT algorithm (Teuler 2007) with M^3 points, where $M = 300$. To improve the accuracy of the calculation, we reduced the frequency content at high frequencies, by considering a square source with an area given by $0.01l^2$. Also, we considered that the source was emitting energy from $t_0 = -0.05\tau$ to $t_f = 0.05\tau$. If we define Δx, Δy, Δt as the distances and times between the points of the 3-D FFT, then the source has a size given by $(2\Delta x) \times (2\Delta y)$ and the source emits energy from $t_0 = -\Delta t$ to $t_f = \Delta t$.

Results of the inversion are plotted in Fig. 3, where the 2-D distribution of the normalized energy density $\bar{I}(\mathbf{r}, t)/(W/l^2)$ is shown as a function of the normalized lengths x/l and y/l. Also the time has been normalized by considering the mean free time t/τ. All the graphics belong to a single 3-D FFT computation. The evolution from ballistic to diffusive behaviour and the effects of a anisotropic source are clearly visualized. Note that, from Fig. 2(b), the backscattered energy in the first scattering event is not directed towards the origin, and as a consequence, a ring of energy may be observed around the origin for quite a long time (see Figs 3a–c). Note also that the anisotropy of the distribution is still evident in Fig. 3(f).

Fig. 4 plots the time variations of intensity at different locations defined by $(r\cos(\alpha), r\sin(\alpha))$, for $r = 1.27l$, $2.53l$, $3.80l$ and $5.06l$ and $\alpha = 0, 45^\circ, 90^\circ$. As expected, the backscattering structure of the indicatrix function and the anisotropy of the source make the time traces to follow a different behaviour depending on the radial distance and angle. In Fig. 4, for $r = 1.27l$, it is possible to observe the passing of the energy ring produced by the backscattering structure of the indicatrix function. Note that in this numerical example, we have considered a source of finite extent emitting a finite amount of energy in a certain amount of time. Then, the envelope does not take infinite values, and its behaviour should be closer to a 'real' case. It is interesting to focus on the behaviour of the envelope near the direct-wave arrival and to explain it by taking into account the forward scattering properties of the indicatrix function in Fig. 2(b). In Fig. 4, it can be observed that the part of the envelope corresponding to the direct-wave arrival broadens as lapse time increases. This can be observed for every value of α. This fact is easily interpreted by noting that our indicatrix function in Fig. 2(b) takes small values for relatively small angles. Then, forward scattered energy is mainly scattered with small angles giving rise to a tail that broadens with time. There are important studies on the subject of envelope broadening (Sato & Fehler, 1998).

Now we will compare the time traces obtained in our numerical example with traces corresponding to cases in which the source or/and the scattering processes are isotropic. The calculations of these new cases are also performed by using the same procedure (3-D FFT algorithm). This is a different way to show the importance of taking into account both the anisotropy of the source and the scattering processes. For this purpose, we have performed the following comparisons, where the anisotropies are still the ones defined in Fig. 2.

5.1 Comparison of anisotropic source and anisotropic scattering case with isotropic source and anisotropic scattering case

Results are shown in Figs 5(a)–(c). In this case, the differences between the results come only from the anisotropy of the source. First of all, we note that the time trace for $r = 0l$ coincides in both cases. It seems then that the amount of scattered energy towards the origin does not depend on the anisotropy of the source. In Fig. 5(b), it is notable that for $\alpha = 45^\circ$, results are completely the same in both cases. The origin of this coincidence is that the anisotropy of the source is described by a cosine square function and $\langle\cos^2(\theta)\rangle = \cos^2(45^0)$; this means that in both cases the same amount of energy is emitted in the direction $\alpha = 45^\circ$. Some differences can be seen in Fig. 5(a), but much bigger differences may be observed between the two traces in the directions in which a small amount of energy or no energy is emitted, as in Fig. 5(c). Because of the anisotropy of the source, no energy is emitted in the direction $\alpha = 90^\circ$. The accumulation of energy due to scattering at small angles explains the existence of a small peak of energy for short times. Broadening of the part of the envelope corresponding to direct arrival happens in both traces for the three graphics.

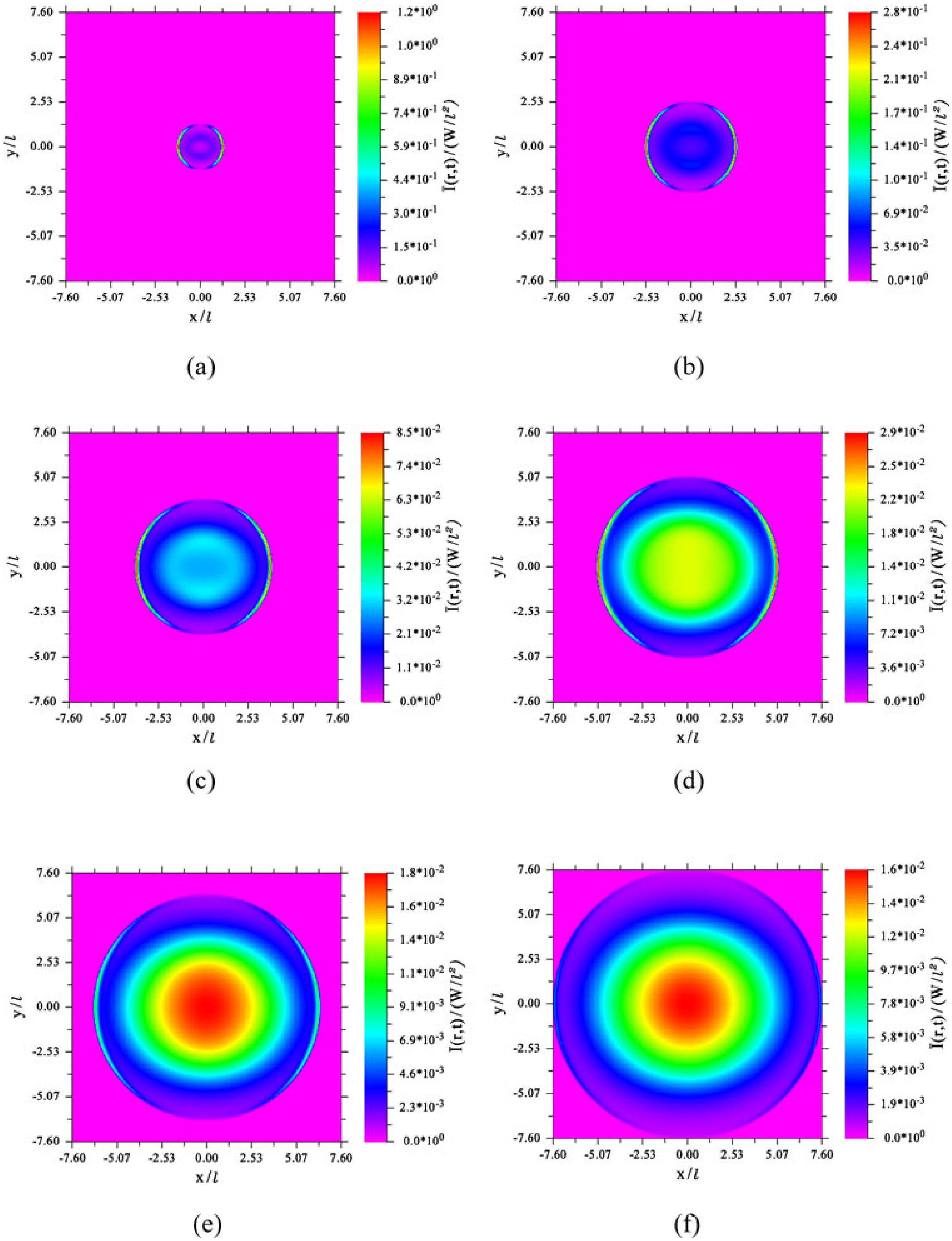

Figure 3. Space–time evolution of the normalized function $\overline{I}(\mathbf{r}, t)/(W/l^2)$. Each figure corresponds to an area of $7.60l \times 7.60l$ and to a different lapse time: (a) $t = 1.27\tau$; (b) $t = 2.53\tau$; (c) $t = 3.80\tau$; (d) $t = 5.06\tau$; (e) $t = 6.34\tau$ and (f) $t = 7.60\tau$. The values of $\overline{I}(\mathbf{r}, t)/(W/l^2)$ are indicated by a different colour/grey scale.

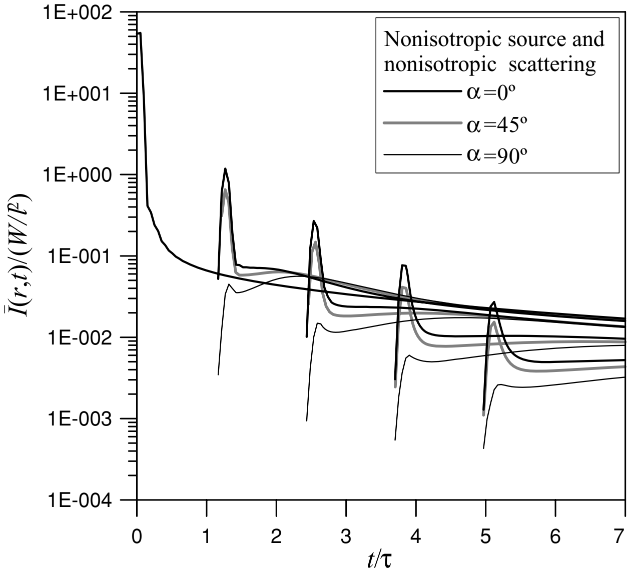

Figure 4. Time traces for a case in which the source is anisotropic and scattering is an anisotropic process (see Fig. 2). The time traces correspond to points located at ($r\,\cos(\alpha)$, $r\,\sin(\alpha)$) for $r = 1.27l$, $2.53l$, $3.80l$ and $5.06l$ and $\alpha = 0$ (black thick line), 45° (grey line) and 90° (black thin line). Note the envelope broadening of the onset as r increases.

5.2 Comparison of anisotropic source and anisotropic scattering case with non-isotropic source and isotropic scattering case

Results are shown in Figs 6(a)–(c). In this case, the differences come only from the scattering process, and the source has the same anisotropic behaviour. It is very interesting to note the envelope broadening of the onset in the anisotropic scattering case in contrast with the isotropic scattering case (see Figs 6a and b). In the anisotropic scattering case, all the time traces have less energy after the onset. In the case $r = 1.27l$, there is a clear secondary maximum. It corresponds to the ring of energy due to the backscattering structure of the indicatrix function already noted in Fig. 3. Note in Fig. 6(c) that the isotropic scattering makes easy the accumulation of energy for small lapse time in the direction $\alpha = 90^\circ$.

5.3 Comparison of anisotropic source and anisotropic scattering case with isotropic source and isotropic scattering case

Results are shown in Figs 7(a)–(c). Note the clear differences in the shapes of both the onset and the behaviour of the time traces for longer times in many cases. Differences are stronger for bigger angles (Figs 7b and c) and closer to the source ($r = 0l$ and $r = 1.27l$). The onset shows again envelope broadening when the scattering is anisotropic. It is interesting to compare Figs 7(b) and 5(b). Note that in 7(b), due to the accumulation of scattered energy at small angles, the energy levels of the onset are higher when the scattering is anisotropic. This can be better noted as r increases. It is also interesting to note that Figs 6(b) and 7(b) are nearly identical. This is justified in the same way as we did for Fig. 5(b) (in both cases the grey line corresponds to isotropic scattering and the same amount of energy is emitted at $\alpha = 45^\circ$).

Finally, it is interesting to show that our calculations for the isotropic source and anisotropic scattering are consistent with the solution of the diffusion equation, which is known to become a good approximation for long lapse time. The 2-D solution of the diffusion equation can be written as

$$\bar{I}_{\mathrm{diff}}(r,t) = \frac{W}{l^2}\frac{\mathrm{e}^{-\frac{(r^2/l^2)}{2(t/\tau)}}}{2\pi\,(t/\tau)}. \tag{32}$$

When scattering is anisotropic, this solution becomes more accurate if the mean free path in equation (32) is substituted by the transport mean path l_m, and the mean free time is substituted by the transport mean free time τ_m (Sheng, 1995) as

$$l_m = l\,(1-\psi)^{-1}, \quad \tau_m = \tau\,(1-\psi)^{-1}. \tag{33}$$

In our case, $(1-\psi)^{-1} = 1.27$. In Fig. 8, we can see a good agreement for long lapse time of our solution with the diffusion solution for $r = 1.27l$, $2.53l$, $3.80l$ and $5.06l$.

6 DISCUSSION AND CONCLUSIONS

In this work, we have derived an analytic and exact solution of the radiative transfer equation in the Fourier space, for an arbitrary anisotropic impulsive point-like source and anisotropic scattering events in a 2-D space. The solution has been written in the Fourier space, and it cannot

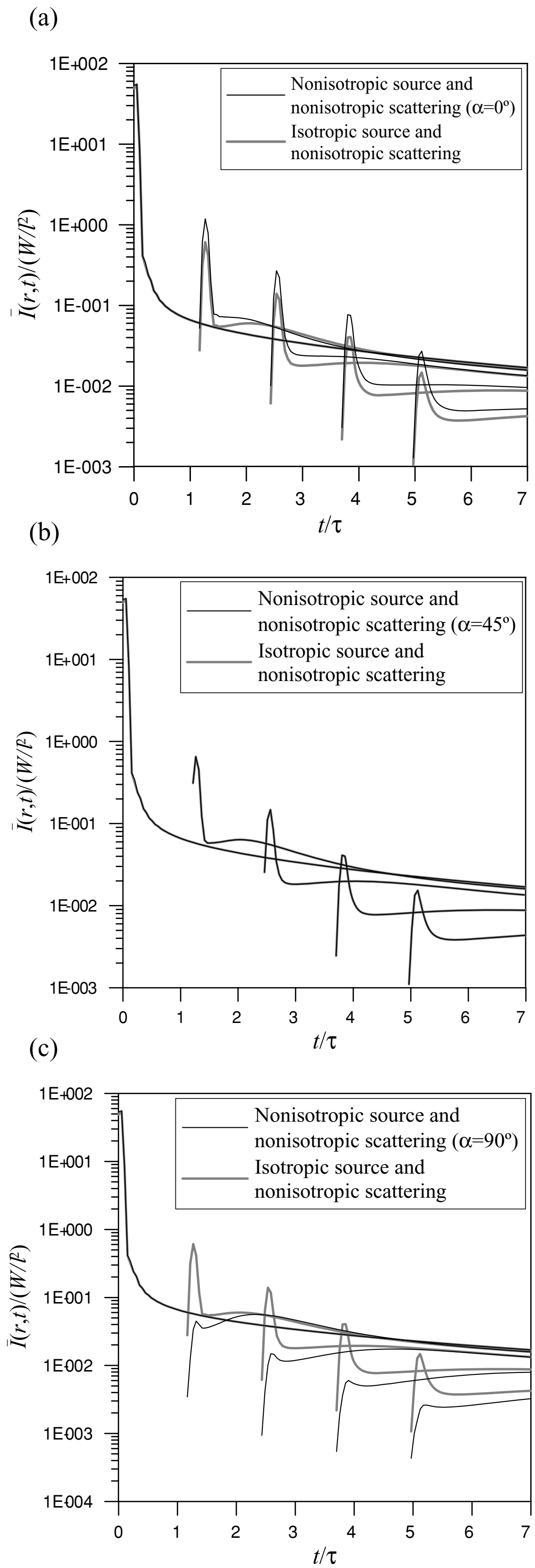

Figure 5. Comparative plot of the results shown in Fig. 4 (black line), with a case in which we consider isotropic source and anisotropic scattering (grey line) for (a) $\alpha = 0$; (b) $\alpha = 45^\circ$ and (c) $\alpha = 90^\circ$.

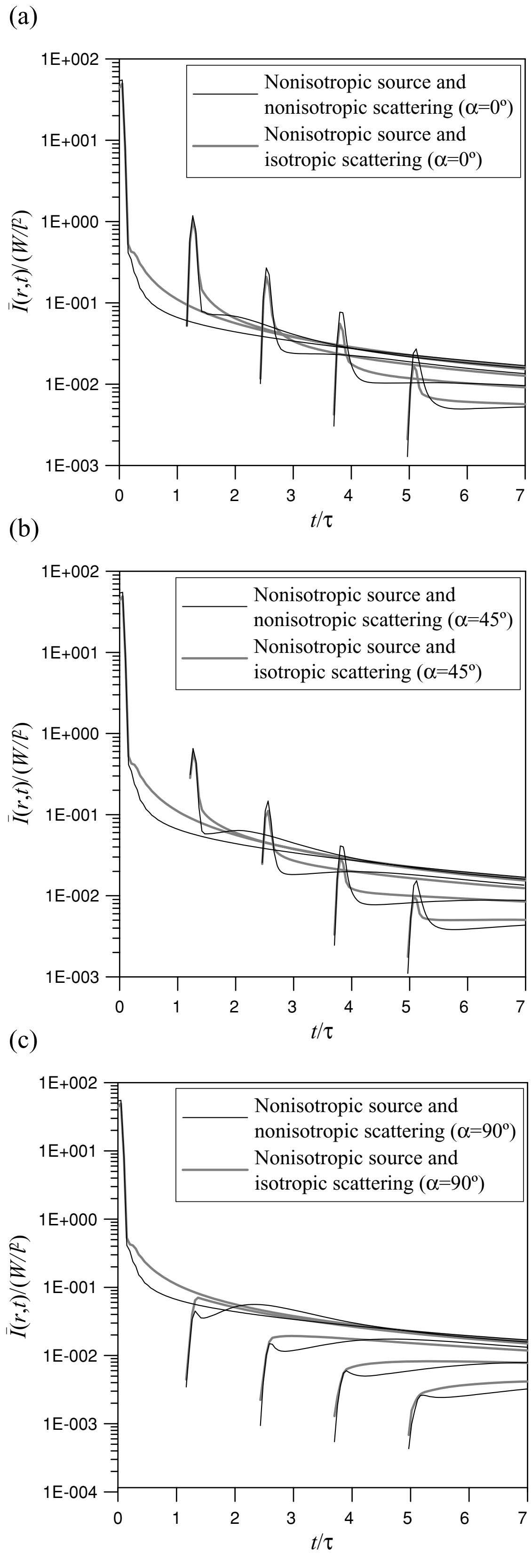

Figure 6. Comparative plot of the results shown in Fig. 4 (black line) with a case in which we consider anisotropic source and isotropic scattering (grey line) for (a) $\alpha = 0$; (b) $\alpha = 45^\circ$ and (c) $\alpha = 90^\circ$.

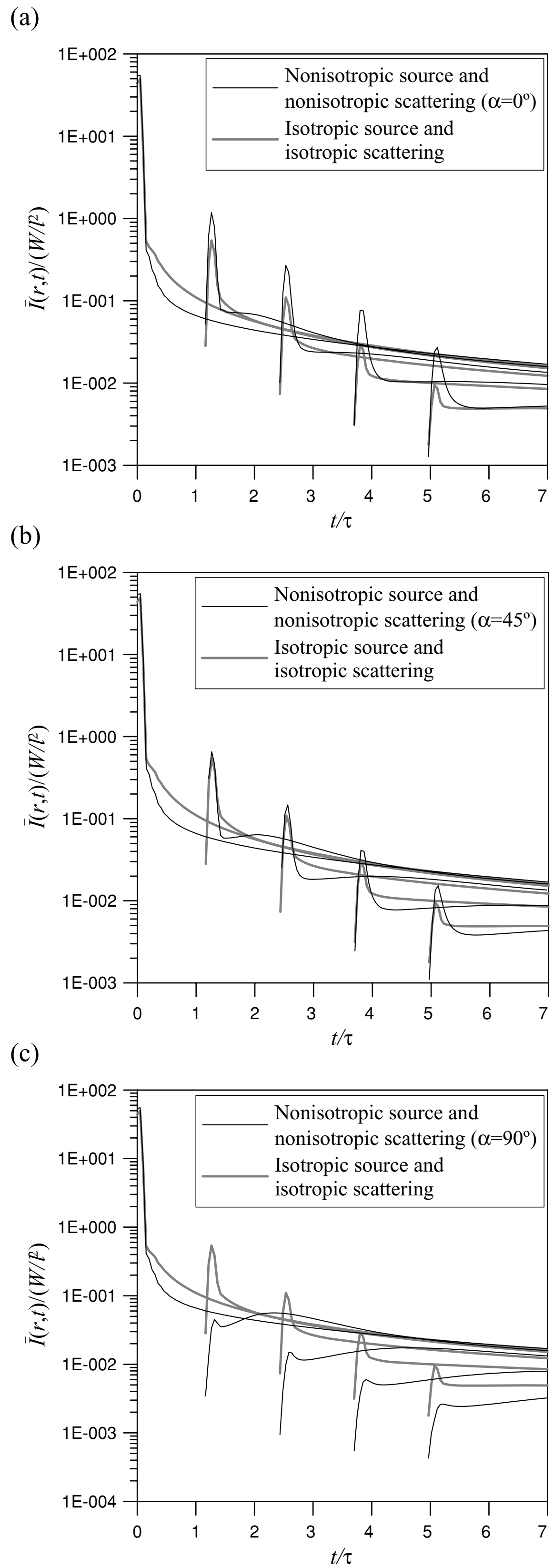

Figure 7. Comparative plot of the results shown in Fig. 4 (black line) with a case in which we consider isotropic source and isotropic scattering (grey line) for (a) $\alpha = 0$; (b) $\alpha = 45^\circ$ and (c) $\alpha = 90^\circ$.

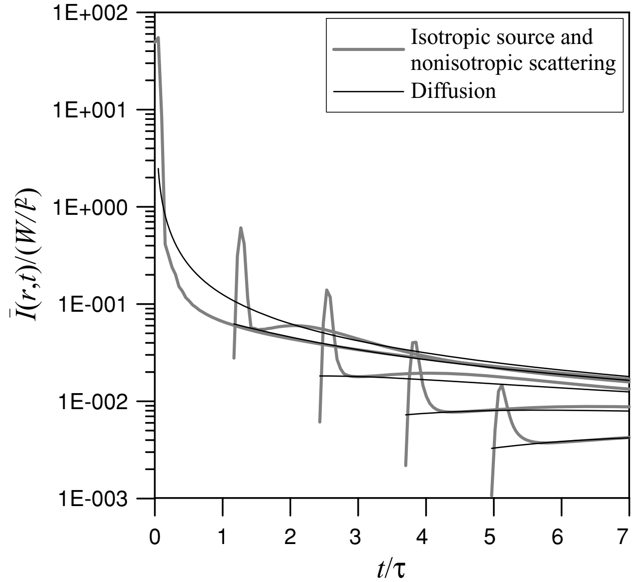

Figure 8. Comparative plot of the results for the case of isotropic source and anisotropic scattering with the 2-D solution of the diffusion equation for $r = 1.27l$, $2.53l$, $3.80l$ and $5.06l$.

be inverted analytically in a general case. If the Fourier series expansion corresponding to the angular dependence of both the source term and the phase function has a finite number of terms, the solution becomes a closed form solution. We have used a fast method to carry out the inversion by using the FFT algorithm to visualize our results in the real space for a particular example. In this example, we considered a anisotropic source and anisotropic scattering events. The shape of the final distribution could be intuitively described from the characteristics of both functions.

From Figs 3 and 4, it becomes evident the importance of the knowledge of anisotropy of both the source and the scattering events to synthesize energy distributions. In this case, the energy distributions become notably different from the isotropic case. In our example, we have shown that it is possible to obtain an accumulation of energy around the origin that looks like a ring of energy. This ring of energy is produced by the single scattering of the ballistic wave. As a consequence, it can only be noted at relative short lapse times, when the ballistic term and the single scattering terms are more important than the contribution of higher order terms. The existence of the ring of energy has been easily justified from the backscattering properties of the indicatrix function. Also, envelope broadening of the direct arrival is observed, and it is justified from the narrow structure of the forward scattering.

Moreover, the source term is anisotropic. The anisotropy of the source is surprisingly noted at every lapse time, even when the distribution shows a diffusive behaviour. The effects of the source term on the distribution of energy can be noted from the angular dependence of the intensity (see Fig. 3). The ballistic term, which is the one that shows a stronger dependence on the anisotropy of the source, shows a greater accumulation of energy near the x-axis. Because of this, the single scattered energy gives rise to an anisotropic ring with more energy near the y-axis (see Fig. 3c). At long lapse times, the distribution has an elliptic shape, showing more energy at the west and east directions for every radial distance. This result can also be justified from the shape of the source term.

Also, we have compared our numerical example with cases in which the source or/and the scattering process are isotropic, and important differences have been shown in many cases. In all the examples, the distances were normalized by using the mean free path, and the times were normalized by using the mean free time. Our development may be used then to compute time traces and energy distributions for any values of the scattering coefficient (inverse of the mean free path) and velocity of propagation. As a conclusion of all our calculations, we point out the importance of taking into account, simultaneously, the anisotropy of both the source term and the indicatrix function (or the phase function).

We believe that this work may be applied to describe scattering and diffusion in 2-D disordered media since it provides a general analytical solution to the radiative transfer equation, which is usually solved by the use of time-consuming numerical techniques or approximated by the use of simple isotropic models. This work may then help further works to fit experimental data to synthetic envelopes to compute important physical or seismological parameters or to carry out inverse analysis when anisotropic sources and anisotropic scattering events are considered.

ACKNOWLEDGMENTS

EC acknowledges a 'Juan de la Cierva' contract and a 'José Castillejo' grant of the Spanish Ministerio de Ciencia y Tecnología (MCYT). This research has been partially supported by the MCYT project CGL-2005-04541-C03-02/BTE. EC also acknowledges the support (both scientific and personal) during a 6 months stay in the Solid Earth Physics Laboratory, Department of Geophysics, Graduate School of Science, Tohoku University, Sendai, Japan. The authors would like to thank H. Sato for his useful suggestions and helpful discussion on the manuscript. The authors are also grateful to the comments of the editor A. Curtis and an anonymous reviewer that further improved this paper.

REFERENCES

Abramowitz, A. & Stegun, I.A., 1970. *Handbook of Mathematical Functions*, Dover, New York.

Abubakirov, I.R., 2005. Attenuation characteristics of transverse waves in the lithosphere of Kamchatka estimated from observations at the Petropavlovsk digital broadband station, *Izvestiya, Phys. Solid Earth,* **41,** 813–824.

Aki, K. & Chouet, B., 1975. Origin of coda waves: source, attenuation and scattering effects, *J. geophys. Res.,* **80,** 3322–3342.

Boguna, M., Porra, J.M., Masoliver, J. & Weiss, G.H., 1996. Isotropization time for non-Markovian CTRW's, *Physica A,* **230,** 149–155.

Born, M. & Wolf, E., 2002. *Principles of Optics*, Cambridge University Press, Cambridge.

Brigham, E., 1998. *Fast Fourier Transform and Its Applications*, Prentice-Hall Inc., Upper Saddle River.

Chandrasekhar, S., 1960. *Radiative Transfer*, Dover, London.

Gusev, A.A. & Abubakirov, I.R., 1987. Monte Carlo simulation of record envelope of a near earthquake, *Phys. Earth planet. Inter.,* **49,** 30–36.

Gusev, A.A. & Abubakirov, I.R., 1996. Simulated envelopes of anisotropically scattered body waves as compared to observed ones: another manifestation of fractal heterogeneity, *Geophys. J. Int.,* **127,** 49–60.

Hoshiba, M., 1991. Simulation of multiple scattered coda wave excitation based on the energy conservation law, *Phys. Earth planet. Int.,* **67,** 123–136.

Hoshiba, M., 1995. Estimation of anisotropic scattering in western Japan using coda wave envelopes: application to a multiple anisotropic scattering model, *J. geophys. Res.,* **100**(B1), 645–657.

Ishimaru, A., 1978. *Wave Propagation and Scattering in Random Media*, Academic Press, New York.

Margerin, L., Campillo, M. & Van Tiggelen B.A., 2000. Monte Carlo simulation of multiple scattering of elastic waves, *J. geophys. Res.,* **105**(B4), 7873–7892.

Paasschens, J.C.J., 1997. Solution of the time-dependent Boltzmann equation, *Phys. Rev. E,* **56,** 1135–1141.

Przybilla, J., Korn, M. & Wegler, U., 2006. Radiative transfer of elastic waves versus finite difference simulations in two-dimensional random media, *J. geophys. Res.,* **111,** B04305, doi:10.1029/2005JB003952.

Rytov, S.M., Kravtsov, Y.A. & Tatarskii, V.I., 1987. *Principles of Statistical Radiophysics*, Vol. **4**, Springer-Verlag, Berlin.

Ryzhick, L., Papanicolau, G. & Keller J.B., 1996. Transport equations for elastic and other waves in random media, *Wave Motion,* **24,** 327–370.

Sato, H., 1994. Formulation of the multiple anisotropic scattering process in 2-D space on the basis of the energy-transport theory, *Geophys. J. Int.,* **117,** 727–732.

Sato, H., 1995. Formulation of the multiple anisotropic scattering process in 3-D space on the basis of the energy-transport theory, *Geophys. J. Int.,* **121,** 523–531.

Sato, H. & Fehler, M.C., 1998. *Seismic Wave Propagation and Scattering in the Heterogeneous Earth*, AIP Series in Modern Acoustics and Signal Processing, Springer-Verlag, New York.

Sato, H., Nakahara, H. & Ohtake, M., 1997. Synthesis of scattered energy density for non-spherical radiation from a point shear dislocation source based on the radiative transfer theory, *Phys. Earth planet. Inter.,* **104,** 1–13.

Shang, T. & Gao, L., 1988. Transportation theory of multiple scattering and its application to seismic coda waves of impulsive source, *Scientia Sinica (Ser. B, China),* **31,** 1503–1514.

Sheng P., 1995. *Introduction to Wave Scattering, Localization, and Mesoscopic Phenomena*, Academic Press, Tokyo.

Takahashi, T., Sato, H., Nishimura, T. & Obara, K., 2007. Strong inhomogenetiy beneath Quaternary volcanoes revealed from the peak delay analysis of *S*-wave seismograms of microearthquakes in northeastern Japan, *Geophys. J. Int.,* **168,** 90–99.

Teuler, J.M., 2007. *JMFFTLIB: A FFT package*, CNRS-France, available at http://www.idris.fr/data/publications/JMFFT/.

Wu, R.-S., 1985. Multiple scattering and energy transfer of seismic waves–separation of scattering effect from intrinsic attenuation, I: theoretical modeling, *Geophys. J. R. astr. Soc.,* **82,** 57–80.

Wu, R.-S. & Aki, K., 1988. Multiple scattering and energy transfer of seismic waves – separation of scattering effect from intrinsic attenuation, II: application of the theory to Hindu-Kush region, *Pure appl. Geophys.,* **128,** 49–80.

Yoshimoto, K., 2000. Monte Carlo simulation of seismogram envelopes in scattering media, *J. geophys. Res.,* **105**(B3), 6153–6161.

Zeng, Y., Su, F. & Aki, K., 1991. Scattered wave energy propagation in a random isotropic scattering medium, I: theory, *J. geophys. Res.,* **96,** 607–619.

APPENDIX

To integrate over the angles, we first define the function $\rho(\mathbf{r}\,|\theta_N, N, \mathbf{L}_N)$

$$\rho(\mathbf{r}\,|\theta_N, N, \mathbf{L}_N) = 2\pi \int_{-\pi}^{\pi} \mathrm{d}\theta_0 \cdots \int_{-\pi}^{\pi} \mathrm{d}\theta_{N-1} \times \prod_{j=0}^{N} \phi_j \left(\theta_j - \theta_{j-1}\right) \delta\left(x - \sum_{j=0}^{N} r_j \cos\theta_j\right) \delta\left(y - \sum_{j=0}^{N} r_j \sin\theta_j\right), \tag{A1}$$

where $\mathbf{L}_N = (r_0, ..., r_j, ..., r_N)$ is a set of constant numbers while performing the integral in (A1). The result of the integration of eq. (A1) will be put into (16) and then the integration over the radial coordinates will be performed.

To calculate $\rho(\mathbf{r}\,|\theta_N, N, \mathbf{L}_N)$, eq. A1, it is convenient to write the product of ϕ_j functions in (A1) as

$$\prod_{k=0}^{N} \phi_k \left(\theta_k - \theta_{k-1}\right) = \frac{1}{(2\pi)^{(N+1)}} \sum_{n_0,\ldots,n_N} \left(\prod_{k=0}^{N} A_{n_k}\right) \mathrm{e}^{\mathrm{i}\left[\sum_{j=0}^{N-1} (n_j - n_{j+1})\theta_j + n_N\theta_N\right]}. \tag{A2}$$

Then, the integrals involving the angles θ_j in eq. (A1) are readily evaluated by using (A2), by taking into account the complex integral definition of the Bessel functions $J_n(x) = (\mathrm{i}^n/2\pi)\int_{-\pi}^{\pi} \exp(-\mathrm{i}x\cos\theta + \mathrm{i}n\theta)\mathrm{d}\theta$ and by writing the delta functions as Fourier transforms in polar coordinates $\delta(x - \sum_{j=0}^{N} r_j \cos\theta_j)\delta(y - \sum_{j=0}^{N} r_j \sin\theta_j) = \frac{1}{(2\pi)^2}\int_0^{\infty} \xi\mathrm{d}\xi \int_{-\pi}^{\pi} \mathrm{d}\varphi \mathrm{e}^{\mathrm{i}\xi r\cos(\theta-\varphi)} \mathrm{e}^{-\mathrm{i}\sum_{j=0}^{N} \xi r_j \cos(\theta_j - \varphi)}$, where the pair $\xi = (\xi, \varphi)$

are the radial and angular coordinates in the Fourier space and $(x, y) = (r\cos\theta, r\sin\theta)$. Therefore, we obtain

$$\rho(\mathbf{r}\,|\theta_N, N, \mathbf{L}_N) = \frac{1}{(2\pi)^2}\int_0^\infty \xi\,\mathrm{d}\xi \int_{-\pi}^{\pi} \mathrm{d}\varphi\, \mathrm{e}^{\mathrm{i}\xi r\cos(\theta-\varphi)}\tilde{\rho}(\xi\,|N, \mathbf{L}_N), \tag{A3}$$

where $\tilde{\rho}(\xi\,|\theta_N, N, \mathbf{L}_N)$ is the Fourier transform of $\rho(\mathbf{r}\,|\theta_N, N, \mathbf{L}_N)$, and it is given by

$$\begin{aligned}\tilde{\rho}(\xi\,|\theta_0, N=0, \mathbf{L}_0) &= \sum_{n_0} P_{n_0}(\xi r_0, \theta_0, \varphi),\\ \tilde{\rho}(\xi\,|\theta_N, N, \mathbf{L}_N) &= \sum_{n_0,\ldots,n_N}\prod_{k=0}^{N-1} Q_{n_k-n_{k+1}}(\xi r_k, \varphi) P_{n_N}(\xi r_N, \theta_N, \varphi)\end{aligned} \tag{A4}$$

and

$$\begin{aligned}Q_{n_j-n_{j+1}}(\xi r_j, \varphi) &= A_{n_j} J_{n_j-n_{j+1}}(\xi r_j)\mathrm{e}^{\mathrm{i}(n_j-n_{j+1})(\varphi-\pi/2)},\\ P_{n_N}(\xi r_N, \theta_N, \varphi) &= A_{n_N}\mathrm{e}^{-\mathrm{i}\xi r_N\cos(\theta_N-\varphi)}\mathrm{e}^{\mathrm{i}n_N\theta_N}.\end{aligned} \tag{A5}$$

We integrate now the radial coordinates in (16). First, we rewrite (16) by using (A1)

$$I(\mathbf{r}, t, \theta_N, N) = \tau\prod_{i=0}^{N}\int_0^\infty \mathrm{d}r_i\, p(r_i)\rho(\mathbf{r}\,|\theta_N, N, \mathbf{L}_N)\delta\left(t - \sum_{i=0}^{N}\frac{r_i}{v}\right). \tag{A6}$$

To solve the integral (A6), we write the delta function as a Fourier transform: $\delta(t - v^{-1}\sum_{j=0}^{N} r_j) = \frac{1}{2\pi}\int_{-\infty}^{\infty}\mathrm{e}^{\mathrm{i}\omega t}\mathrm{e}^{-\mathrm{i}\omega v^{-1}\sum_{j=0}^{N} r_j}\mathrm{d}\omega$, where ω is the corresponding temporal coordinate in the Fourier space. Then we use eqs (A3) and (A4) into (A6) and integrate the set of variables $\mathbf{L_N}$. We obtain

$$I(\mathbf{r}, t, \theta_N, N) = \frac{1}{(2\pi)^3}\int_{-\infty}^{\infty}\mathrm{e}^{\mathrm{i}\omega t}\mathrm{d}\omega\int_0^\infty \xi\,\mathrm{d}\xi\int_{-\pi}^{\pi}\mathrm{d}\varphi\,\mathrm{e}^{\mathrm{i}\xi r\cos(\theta-\varphi)}\tilde{I}(\xi, \omega, \theta_N, N), \tag{A7}$$

where $\tilde{I}(\xi, \omega, \theta_N, N)$ is the Fourier transform of $I(\mathbf{r}, t, \theta_N, N)$, and it is given by

$$\begin{aligned}\tilde{I}(\xi, \omega, \theta_0, N=0) &= \tau\sum_{n_0} E_{n_0}(\xi, \omega, \theta_0),\\ \tilde{I}(\xi, \omega, \theta_N, N) &= \tau\sum_{n_0,\ldots,n_N}\prod_{k=0}^{N-1} C_{n_k-n_{k+1}}(\xi, \omega)E_{n_N}(\xi, \omega, \theta_N),\ N > 0\end{aligned} \tag{A8}$$

and

$$\begin{aligned}E_{n_N}(\xi, \omega, \theta_N) &= \int_0^\infty \mathrm{d}r_N\, p(r_N)P_{n_N}(\xi r_N, \theta_N, \varphi)\mathrm{e}^{-\mathrm{i}\frac{\omega}{v}r_N},\\ C_{n_j-n_{j+1}}(\xi, \omega) &= \int_0^\infty \mathrm{d}r_j\, p(r_j)Q_{n_j-n_{j+1}}(\xi r_j, \varphi)\mathrm{e}^{-\mathrm{i}\frac{\omega}{v}r_j}.\end{aligned} \tag{A9}$$

We will solve now the integrals (A9) analytically. Using eq. (11) into (A9), we obtain

$$\begin{aligned}E_{n_N}(\xi, \omega, \theta_N) &= l^{-1}A_{n_N}\mathrm{e}^{\mathrm{i}n_N\theta_N}\int_0^\infty \mathrm{d}r_N\,\mathrm{e}^{-\{l^{-1}+\mathrm{i}[\omega/v+\xi\cos(\theta_N-\varphi)]\}r_N},\\ C_{n_j-n_{j+1}}(\xi, \omega) &= l^{-1}A_{n_j}\mathrm{e}^{\mathrm{i}(n_j-n_{j+1})(\varphi-\pi/2)}\int_0^\infty \mathrm{d}r_j\, J_{n_j-n_{j+1}}(\xi r_j)\mathrm{e}^{-(l^{-1}+\mathrm{i}\omega/v)r_j}.\end{aligned} \tag{A10}$$

The integral for $E_{n_N}(\xi, \omega, \theta_N)$ can be easily solved and by recognizing that the integral for $C_{n_j-n_{j+1}}(\xi, \omega)$ corresponds to the Laplace transform of a Bessel function (Abramowitz & Stegun 1970), we readily write

$$\begin{aligned}E_{n_N}(\xi, \omega, \theta_N) &= \frac{\tau^{-1}A_{n_N}\mathrm{e}^{\mathrm{i}n_N\theta_N}}{\tau^{-1}+\mathrm{i}\,[\omega + v\xi\cos(\theta_N-\varphi)]},\\ C_{n_j-n_{j+1}}(\xi, \omega) &= A_{n_j}\mathrm{e}^{\mathrm{i}(n_j-n_{j+1})(\varphi-\pi/2)}D_{n_j-n_{j+1}}(\xi, \omega),\end{aligned} \tag{A11}$$

where the function D_n is defined as

$$\begin{aligned}D_n(\xi, \omega) &= \tau^{-1}\frac{\left[\sqrt{(\tau^{-1}+\mathrm{i}\omega)^2 + v^2\xi^2} - \left(\tau^{-1}+\mathrm{i}\omega\right)\right]^n}{v^n\xi^n\sqrt{(\tau^{-1}+\mathrm{i}\omega)^2+v^2\xi^2}}\ ,\ n > -1,\\ D_{-n}(\xi, \omega) &= (-1)^n D_n(\xi, \omega)\,,\ n < 0\,.\end{aligned} \tag{A12}$$